Effect of slam force duration on the vibratory response of a light weight high speed wave piercing catamaran

J J McVicar[1], J Lavroff[1], M R Davis[1], G A Thomas[2]

[1]University of Tasmania, Australia

[2]University College London, UK

Abstract

When the surface of a ship meets the water surface at an acute angle with a high relative velocity, significant short duration forces can act on the hull plating. Such an event is referred to as a slam. Slam loads imparted on ships are generally considered to be of an impulsive nature. As such, slam loads induce vibration in the global hull structure which has implications for both hull girder bending strength and fatigue life of a vessel. A modal method is often used for structural analysis whereby higher order modes are neglected to reduce computational effort.

The effect of the slam load temporal distribution on the whipping response and vertical bending moment are investigated here using a continuous beam model with application to a 112 m INCAT wave piercing catamaran and correlation to full scale and model scale experimental data. Experimental studies have indicated that the vertical bending moment is dominated by the fundamental longitudinal bending mode of the structure. However, it is shown here that although the fundamental mode is dominant in the global structural response, the higher order modes play a significant role in the early stages of the response and may not be readily identifiable if measurements are not taken sufficiently close to the slam location. A relationship between the slam duration and the relative modal response magnitudes is found which is useful in determining the appropriate truncation of a modal solution.

Nomenclature

A = Cross sectional area (m^2)

b = Modal mass scaling (m^3)

c = Arbitrary constant

d_v = Vessel draft (m)

E = Material modulus of elasticity (Pa)

f = Frequency (Hz)

$\hat{f}$ = Peak force magnitude (N)

F = Transient slam force (N)

g = Acceleration due to gravity (m s^{-2})

h = Transverse beam deflection (m)

$h_{\max}$ = Peak displacement (m)

H = Mode shape transverse deflection amplitude (m)

I = Second moment of area (m^4)

J = Impulse magnitude (Ns)

$\hat{k}$ = Elastic base stiffness per unit length (N m^{-2})

L = Beam length (m)

L_{WL} = Waterline Length (m)

m_a = Water added mass (kg)

m_n = Modal mass (kg)

m_v = Vessel displacement (kg)

n = Mode index

N = Modal truncation number

p = Hydrodynamic force distribution (N m^{-1})

q = Modal displacement

Q = Modal force (N)

r = Ramping fraction

t = Time (s)

t_0 = Start time of slam force (s)

t_1 = End time of slam force (s)

Δt_r = Ramping time (s)

T = Modal period (s)

u = Unit step or Heaviside function

x = Spatial variable – distance from transom (m)

β = Wave number (m^{-1})

δ^* = Force-normalised peak displacement

ϵ^* = Step response overshoot

η^* = Impulse-normalised peak displacement

ζ = Damping ratio

ρ = Density (kg m^{-3})

τ = Dimensionless time

ω = Angular frequency (rad s^{-1})

1. Introduction

For the efficient operation of high speed craft it is critical that the vessel mass be minimised to improve speed and efficiency without compromising the structural strength. To do so the operating loads acting on the structure need to be accurately estimated. When operating in rough seas, the significant relative motion between the vessel and the water surface can result in the hull encountering the water surface at an acute angle imparting impulsive loads to the hull (Faltinsen, et. al., 2004). The impulsive event, referred to as a slam, excites the hull structure causing structural vibration. Kapsenberg (2011) states that the slamming problem can be subdivided into a local problem, including a subset of the ship structure in the vicinity of the slam impact, and a problem of the global response of the hull girder. Of interest here is the global longitudinal vibration of the hull girder, known as whipping.

In the catamaran hull form the wet-deck, which is the horizontal structure connecting the two demihulls, presents a large flat surface which is susceptible to extreme slam events. Wet-deck slam loads can be so large that the imparted impulsive load results in the greatest longitudinal bending strength requirement for the vessel (Lavroff et al., 2010 and Thomas et. al., 2003). Further reinforcing the significance of the slam loads is the requirement by class societies to provide first principles derivations of the loads acting on high speed catamarans greater than 100 m in

length (DNV, 2011). Ge et al. (2005) presented a method for estimation of wet-deck slam loads on a conventional catamaran and demonstrated fair agreement to experimental work. In contrast to the conventional catamaran, the wave piercing catamaran hull form, shown in Fig. 1, introduces a centre bow to reduce the horizontal surface area and provide a progressive water entry. In extreme conditions, however, slamming can still occur once the centre bow is fully immersed. The significant geometric features of a wave piercing catamaran are presented in Fig. 2.

The slamming process in wave piercing catamarans is quite unlike that of any other type of vessel. In the most extreme slam events, the first phase of the slam is a bottom slam on the forward section of the demihulls. From a global perspective, the demihull bottom slam is of little consequence, due to the relatively small surface area of the demihulls. This is followed by entry of the centre bow during which jet flows are formed by both the centre bow and the demihulls as the arch ways between the centre bow and demihull segments fill. At the time of arch filling a final very rapid peak in the slam force is observed. The multiple events in the overall slam impart energy to the structure on multiple time scales. This general process has been documented by Lavroff et al., 2011; Amin, 2009 and Shahraki, 2014. Wave piercing catamarans are relatively stiff in bending owing to the overall height of the structure relative to the length with a ratio of approximately 1:5. As a consequence the two node bending frequencies are relatively high being around 2.4 Hz for a 112 m vessel (Amin et al., 2014) and with damping ratios around 0.05 (Thomas et al., 2008). Table 1 compares the mass, stiffness and slam duration of a 112m INCAT catamaran to those of several other monohull vessels. The parameters have been scaled as necessary to full scale equivalent values and the slam duration has been estimated from transient plots presented in each of the papers. Normalising the sectional moment of areas (I) and the vessel displacements (m_v) by the vessel lengths (to the power of 4 and 3 respectively) shows that the INCAT catamaran is relatively much lighter and stiffer, resulting in significantly higher vertical bending mode frequencies; unsurprising given that the INCAT catamaran is all aluminium construction and is significantly stiffened by the presence of the two demihulls. Thus, whipping occurs at a much higher frequency (about 2.4 Hz) than the wave encounter frequency at which peak slamming occurs, approximately 0.23 Hz. Wet deck slam loads are substantial with peak slam forces of the order of the vessel weight (Amin et al., 2009). Furthermore, for wave piercing catamarans the slam excitation and global vibration response have similar time scales allowing significant energy to be transferred to whipping vibrations which follow slam events. As there is similarity in the time scales, quantifying the slam impulse alone is insufficient as the temporal variation in slam force can significantly affect the structural response.

The complex fluid structure interaction present during slam events often necessitates the separation of the fluid and structural solutions. This requires assumptions to be made over the nature of the fluid forcing and can lead to significant errors in the predicted slam loads and structural stresses (Das and Cheung, 2012). In order to accurately capture the non-linearity present during slam conditions, numerical simulations are receiving increased attention (Castiglione et. al. 2011). Finite element methods are commonly used to model the ship structure which can be computationally expensive for transient simulations. If the global bending stresses in the hull girder are of interest, the structural solution can be performed on a modal basis using a restricted set of low frequency modes. In such cases, the local stresses in the hull plating and frame must then be estimated separately. As slam events are of relatively short duration the participation of higher order modes in the whipping response could be expected. It is therefore necessary to determine an appropriate truncation point to ensure that the global bending moment and shear force distributions are correctly estimated.

Cheung et al. (1998) demonstrated that for the SWATH (small waterplane area twin hull) form, the high frequency modes may be necessary, even in non-slamming conditions, to correctly identify effects of local stress concentrations. Bishop and Price (1979) investigated the modal convergence for the symmetric response under non-slamming conditions and concluded that truncation of the solution to 3 flexural modes is typically adequate for conventional ships, while inclusion of 6 flexural modes is conservative. However, high speed catamarans are relatively stiff in bending and these conclusions for conventional ship hulls do not necessarily apply in the case of catamaran ferries. In non-slamming conditions, the spatial variation of the hydrodynamic loading is on the scale of the wavelength. As the wavelengths become small relative to the ship length, the wave height decreases such that the spatial variation is small. However, slamming loads can be rapid and highly localised allowing significant energy to be imparted to the higher order modes and the modal convergence under such conditions needs to be considered in the broad context of light weight catamaran ferries.

A wet-deck slam event was recorded on a 112m INCAT catamaran during a Bass Strait crossing during the delivery voyage (hull 064, shown in Fig. 1). The transient record from an accelerometer mounted at the bow is shown in Fig. 3 (Lavroff et al., 2009). The resultant whipping vibrations are dominated by decaying oscillation at 2.4 Hz, which coincides with the fundamental longitudinal vibration modal frequency as estimated by Amin et al. (2014) using finite element analysis for a similar vessel. Fourier and continuous wavelet transform of the signal

reveals smaller magnitude accelerations at higher frequencies, as shown in Fig. 4. This suggests that the slam impulse imparts energy to the higher modes also.

The slamming behaviour of the 112 m INCAT vessel has previously been investigated at model scale using hydroelastic segmented models (Lavroff, 2009; Amin, 2009; Matsubara, 2011; French, 2012; Shahraki, 2014). Fig. 5 (Lavroff, J., 2009b) shows a 2.5 m long model with a displacement of 27 kg during centre bow entry. Jet flows can be seen to form on the centre bow and demihulls and meet at the top of the arch. During water entry the centre bow produces an upward force as a result of both buoyant and hydrodynamic forces. Confluence of the jets formed during demihull and bow entry and eventual filling of the arch result in significant localised loading. At model scale the peak slam force of 230 N was measured which is 87% of the model displacement (Lavroff et. al., 2011). This is consistent with full scale trials where the peak slam load reached 93% of the total vessel weight during trials (Thomas et al., 2003). In the model scale vibration response, structural modes with modal frequencies of more than four times the fundamental frequency have been observed in the whipping response (Lavroff et. al., 2011) demonstrating that the slam is of short duration and that higher order modes can be excited by wet-deck slam events.

In this paper the effect of the temporal slam duration on the whipping response is investigated through a theoretical model representative of a ship. In structural impact testing, the duration of the impact is altered to impart energy to the vibration modes of interest and provide minimal excitation to higher order modes (Waltham and Kotlicki, 2009). Increases of the impact duration reduce the response of high frequency modes. In the same manner, the temporal distribution of the slam load will affect which modes are excited by the slam and participate in the whipping response. Clough and Penzien (1993) provide a brief general summary of the effect of pulse duration in undamped second order systems. The analysis in this paper further considers a continuous system in the context of global ship vibration. A prescribed forcing term is imparted to a structural model of the ship which includes added mass terms. Apart from the added mass terms effects of two-way coupling are not considered, thus the analysis can be classified as a one-way fluid structure interaction. In this context hydroelastic two-way coupling (i.e. hyrdoelasticity) implies that the structural dynamic deformation modifies the overall fluid flow pattern significantly. In the present application the hull vibration does induce added mass effects in the surrounding fluid but is small in displacement relative to the scale of the flow features. Amin (2009) demonstrated that the effects of hydroelasticity on the slam forcing term were insignificant by comparing the slamming pressures and accelerations of a hydroelastic model with flexible links to those with effectively rigid links.

As only the general dynamic behaviour of a ship girder is of interest a uniform beam model is used. Analysis of a ship as an elastic beam is not a new idea and has been a common simplification for some time. For example, McGoldrick (1960) discusses beam theory for ship vibration analysis using a free-free beam, as do Bishop and Price (1979). More recently Timoshenko beam theory has been used by Jang et al. (2007) to estimate steady state vibration of the hull girder in response to wave excitation in non-slamming conditions and by Dessi and Mariani (2008) to predict the structural response of a high speed monohull in slamming conditions. However, here the model is used to consider the effect that variations in the temporal distribution of the slam force have on the hull girder with a primary focus on the slam duration. While a uniform beam model is somewhat abstracted from the reality of a ship encountering waves with significant forward speed, it is utilised to gain understanding of the dynamics involved when a vessel is subject to a variety of impulsive loading conditions which may be experienced during normal operation. The model parameters and impulse characteristics are chosen here to be representative of a typical catamaran ferry hull. A case study of a 112 m INCAT wave piercing catamaran is performed and the effects of force duration and modal truncation on the response are investigated. Three forcing functions are considered: Dirac delta impulse; rectangular pulse and smoothed rectangular pulse. The Dirac delta impulse function is used to observe the effects of the higher order modes when strongly excited. The rectangular and smoothed rectangular pulses provide excitation on multiple time scales, as is the case in the multiple phase slam process in wave piercing catamarans. The time range of interest in this investigation commences at the slam initiation and ends at the time of peak bending response. Over this time period variations in sectional properties, such as added mass, are minimal: as the global bending frequencies of wave piercing catamarans are significantly higher than wave encounter frequencies in slamming conditions. Thus, the temporal variations in sectional properties are neglected.

2. Model

The representative model of the wet ship system is shown in Fig. 6 and consists of an Euler beam of stiffness, EI, and linear density, ρA, to represent the hull girder, resting on an elastic foundation with stiffness per unit length, $\hat{k}$, to represent the hydrostatic forces. An external distributed load, p, acting on the hull girder was considered and used to represent the slam impulse. The governing equation of the system is:

$$\rho A\ddot{h} + EIh^{IV} + \hat{k}h = p \qquad (1)$$

where a superscript roman numeral has been used to denote derivative differentiation with respect to space and an over-dot for differentiation with respect to time. The associated boundary conditions are:

$$h^{\mathrm{II}}\Big|_0^L = 0 \tag{2}$$

$$h^{\mathrm{III}}\Big|_0^L = 0 \tag{3}$$

which represent zero shear force and zero moment at both ends of the beam (free-free). As the modal characteristics in the impulse response were of interest, a modal analysis was performed to extract the mode shapes and frequencies of the system. Using a separation of variables:

$$h(x,t) = q(t)H(x) \tag{4}$$

and assuming simple harmonic motion:

$$q(t) = c\sin\omega t \tag{5}$$

the unforced system can be reduced to:

$$H^{IV}(x) - \beta^4 H(x) = 0 \tag{6}$$

with:

$$\beta^4 = \frac{\rho A\omega^2 - \hat{k}}{EI} \tag{7}$$

Equation 6 is of the same form as a free-free beam without elastic base and thus the mode shapes are those of the simple free-free beam. However, the relationship between the wave-number β and the modal frequencies, Equation 7, is modified by the elastic base stiffness and, hence, the modal frequencies are dissimilar to the simple free-free beam. In the current treatment, the rigid body modes are treated in the same manner as the flexible modes. The modes are thus generalised modes as discussed by Tuitman et al. (2012). The first six modes are presented in Fig. 7.

By the mode superposition principle (Rao, 1995) the equation of motion was decomposed into N decoupled equations describing the system:

$$\rho A \sum_1^N \ddot{q}_n(t) H_n(x) + \sum_1^N \beta^4 E I q_n(t) H(x) + \sum_1^N \hat{k} q_n(t) H_n(x) = p(x,t) \quad (8)$$

The n^{th} decoupled equation is found by multiplying Equation 8 by the n^{th} mode shape, $H_n(x)$, and integrating over the spatial variable, x, from 0 to l:

$$\ddot{q}_n(t) + \omega^2 q_n(t) = \frac{1}{\rho A b_n} Q_n(t) \quad (9)$$

As the mode shapes are orthogonal to one another, only the n^{th} term of the sums in Equation 8 is non-zero. The parameter Q_n is the generalised force:

$$Q_n = \int_0^L H_n(x) p(x) \, \mathrm{d}x \quad (10)$$

The parameter b_n is given by:

$$b_n = \int_0^L H_n(x)^2 \, \mathrm{d}x \quad (11)$$

As a transient analysis is to be performed, it is necessary to introduce damping to the system. Here it is assumed that the damping does not couple the modes and can be applied to each mode individually. Thus, the temporal equation of motion (Equation 9) was modified to include damping and implemented as in Equation 12:

$$\ddot{q}_n(t) + 2\zeta_n\omega_n + \omega^2 q_n(t) = \frac{1}{\rho A b_n} Q_n(t) \quad (12)$$

In the following section this analysis of the transient response to impulsive structural loadings is focused on the particular case of wave slam on the structure of a wave piercing catamaran. Features of interest which distinguish this case are the very rapid nature of the dominant slam loading which occurs when the arches between the centre bow and the main demi-hulls fill and the relatively stiff bending characteristics of the catamaran hull which has a relatively small ratio of the overall structural height to vessel length. The consequence is that both slam loading and bending (or whipping) vibration have short time frames when compared to other classes of vessel. Thus the particular structural response to slamming of a wave piercing catamaran is influenced by the short time frames of excitation and response and so differs significantly from the response encountered in many other ship structures.

3. Model Parameters for a 112m INCAT Wave Piercing Catamaran

The uniform beam model was used to investigate the effects of the slam duration on the response of the longitudinal vertical bending modes of INCAT hull 064, a 112 m wave piercing catamaran. A general arrangement of Hull 064, Natchan Rera, is shown in Fig. 8. Estimates of the mass and stiffness parameters for the uniform beam model were made for the wet ship system. The added mass was treated as constant and equal to 71% of the hull mass as estimated by Amin (2009) for a similar vessel. Temporal variation in added mass is not considered in the present analysis. The temporal variation in added mass occurs on the time scale of the encounter frequency which is significantly longer than the time scale of the vertical bending frequencies in wave piercing catamarans. Thus, any variation in added mass occurring between the peak slam force and peak bending response is expected to be insignificant. The ship particulars are presented in Table 2 as well as the estimated slam impulse magnitude, slam induced vertical bending moment, and dominant slam location in head seas, all being extrapolated from model scale test data gathered by Lavroff (2009b). The slam duration is based on both extrapolation from model scale data gathered by Lavroff (2009b) and full scale data analysed by Amin (2009). The fundamental longitudinal bending frequency was estimated by Lavroff (2009). Table 3 lists the estimated mass and stiffness parameters. Equation 18

was used to calculate the linear density, ρA, from the vessel mass, m_v, added mass, m_a, and the waterline length, L_{WL}:

$$\rho A = \frac{m_v + m_a}{L_{WL}} \tag{18}$$

The elastic base stiffness, $\hat{k}$, was approximated using the dry hull weight, $m_v g$, the vessel draft, d_v, and waterline length as in Equation 19:

$$\hat{k} = \frac{m_v g}{d_v L_{WL}} \tag{19}$$

Finally, the beam stiffness, EI, was selected to match the fundamental bending frequency predicted by the model to the experimentally determined frequency of 2.4 Hz. The mass and stiffness distributions used in the model are compared to finite element estimates for the 112 m catamaran vessel in Fig. 9 and Fig. 10. The mass distribution varies significantly along the vessel with a mean value of 35.4×10^3 kg m^{-1}. There is reduced variation in the stiffness which has a mean value of 2.04×10^{12} Nm^2. Both means are within 3% of the parameters used in the uniform beam model which was established so as to give the correct whipping mode frequency.

A modal analysis was performed to identify the modelled frequencies of the system modes and the first 6 modal frequencies are presented in Table 4. The heave and pitch frequencies are dependent on the system mass and elastic base stiffness. As they are not relevant to the flexural response, they were not matched to experimental data. By parameter selection, the first longitudinal frequency agrees with the experimental measurement.

Thomas et al. (2008) estimated damping ratios experimentally at full scale and investigated the damping mechanisms for two INCAT vessels with overall lengths of 86.6 m and 96 m. The majority of the damping was attributed to structural damping, which accounts for the inherent material damping as well as damping due to structural connections and fit-out. The identified damping ratios for the fundamental longitudinal bending mode were in the range $0.0035 < \zeta < 0.07$. Lavroff et al. (2009) estimated the damping ratios for the fundamental longitudinal bending mode from slam data for 98m and 112m INCAT vessels as $0.017 < \zeta < 0.032$ and $\zeta = 0.065$ respectively. It follows that estimation of accurate damping ratios would be a complicated task and so the direct

overall measurement of the damping ratios by Lavroff and Thomas is taken as the basis here. A damping ratio of $\zeta = 0.05$ was applied to the first five modes and a ratio of $\zeta = 0.1$ was applied to the higher modes. Typically the higher order global modes of ship structures have larger damping ratios, thus the values used were representative of the system. As the damping ratio has a significant effect on the response magnitude, only two damping values are used here such that the effect of force duration on the response was not masked by changes in damping ratio. Effects of variation in the damping ratio were not explicitly investigated.

4. Dirac Delta Function Impulse Response

The response of the system to a Dirac delta impulse was first considered. This ensured that the high order modes would be excited and enable their contribution to global bending moment to be analysed. Two separate impact locations were considered and the effect on both the displacement response and bending moment response was observed. The displacement and bending responses were calculated for truncated modal solutions using N modes. The peak displacement is presented as a function of N in Fig. 11 for an impact at the bow and the dominant wet-deck slam location in head sea conditions. In both cases the heave and pitch modes account for the majority of the global motion and after inclusion of the fundamental bending mode ($N = 3$) the peak displacement is effectively converged. As the Dirac delta function impulse imparts energy to the high frequency modes this shows that even for short impulses, where higher frequency modes are excited, the low order modes remain dominant in the global displacement response.

The estimated spatial deflections at four instants in time following an impact at the dominant slam location are shown in Fig. 12 using truncation numbers of $N = 3$ (1 flexural mode) and $N = 30$ (28 flexural modes). Significant differences between the two solutions are evident immediately after the impact. However, as the motion develops in time the response of the lower order modes becomes dominant. After 0.1s there is little difference between the two solutions. As the higher frequency modes respond more quickly to the onset of the impact they are dominant in the early response but the magnitude of their displacement response is small. Additionally, the high frequency modes decay quickly, as they complete a significant number of cycles over a short period of time. Thus, the lower order modes become increasingly dominant as the transient response unfolds.

It can also be seen in Fig. 12 that the early deflections, which result from the high order modes, are confined to an area close to the impact location. As a result, the presence of higher order modes in the whipping response may only be observable in measurements which are in the vicinity of the slam impulse. Fig. 13 shows the modelled transient bending records at the slam location and at mid ship using a truncation number of $N = 15$. The slam force is here established as a point force; this is a valid approach for a wave piercing catamaran since the arch slam pressure distribution spans a very small longitudinal area, approximately approximately $0.05L_{WL}$ (Amin, 2009), and is approximated here as a point force. Vibration of the higher order modes is clearly observable in the vertical bending moment at the slam location. However, at the mid ship position the bending moment is strongly dominated by vibration of the fundamental bending mode at 2.4 Hz. In experimental data, noise contamination would further mask any presence of the higher order modes.

The peak vertical bending moment response as a function of the truncation number to the Dirac delta function impulse of 9 MNs, extrapolated from model scale results (Lavroff, 2009b), is shown in Fig. 14 for an impact at the bow and at the dominant wet-deck slam location in head sea conditions. Both show a general linear trend with a superimposed oscillatory component for the impact at the dominant slam location due to the proximity of the impact to the system nodes. In contrast to the displacement response, the bending moment response does not converge as the truncation number is increased. The convergence of the system displacement response for the same forcing condition shows that it may be difficult to quantify the modal participation based on the displacement response alone. Any real loading case cannot be of infinitely short duration and the peak bending moment will converge to a finite value as the truncation number is increased. However, this does emphasise that the higher order modes, if excited, can contribute significantly to bending stresses despite their smaller displacement response.

5. Effect of impulse duration on displacement and bending moment response

The duration of the slam force alters the response of the system modes. To isolate the effect of force duration the impulse, $J = \int F\, dt$, was held constant while the force duration was varied. To this end, the transient force function was defined as a rectangular pulse, as represented by Equation 20, and the peak force magnitude was scaled by the force duration; a point force is considered to isolate the temporal effects from spatial effects:

$$F(t) = \frac{\hat{f}}{\Delta t}\big(u(t - t_0) - u(t - t_1)\big) \quad (20)$$

The force duration is represented by Δt; u is the Heaviside step function; and t_0 and t_1 are the times at which the force commences and terminates respectively. The transient displacement response of the system to a rectangular pulse with duration $\Delta t = 0.15$s (the typical slam duration presented in Table 2) is shown in Fig. 15 for modes 3, 4 and 7. We see that modes 4 and 7 have very small displacements compared to mode 3 by factors of 50 and 100 respectively. Three distinct response characteristics are observed. The transient displacement response of mode three (the fundamental bending mode) exhibits an impulse response characteristic of decaying oscillation about zero mean. For mode seven, the rectangular pulse has a significant duration relative to the modal period. As a result, the response of mode seven has step response characteristics where the upward and downward edges of the transient force at times t_0 and t_1 can be considered as separate step response events. Finally, the modal period of mode four is of a comparative time to the rectangular pulse duration and as a result the response of mode four lies in a transitional region; it exhibits neither impulse response nor step response characteristics.

The observed transitional behaviour reveals that for the 112 m INCAT catamaran, only the fundamental bending mode responds with impulse characteristics to an impact with the typical slam duration and the fundamental mode displacement response is very much larger than the higher modes. It is therefore necessary to identify the behaviour of the system through the transitional region to understand the response of each vibration mode to the slam forces. To quantitatively investigate the displacement response as a function of the impact duration, the transient displacement response of each mode was characterised by the peak displacement, $h_{\max,n}$, which occurs in the transient response. The peak displacement is marked for each mode by a cross in Fig. 15.

The effect of the force duration on the peak displacement of modes 3, 6, 9 and 12 is shown in Fig. 16. All modes exhibit a reduction in peak displacement for increased force durations, with the reduction occurring at higher rates for the higher frequency modes. The relationship can be better understood by non-dimensionalising the parameters. The force duration was non-dimensionalised using the modal undamped natural period, T_n, as in Equation 21:

$$\tau_n = \frac{\omega_n \Delta t}{2\pi} = \frac{\Delta t}{T_n} \quad (21)$$

Two different dimensionless forms of the peak displacement were considered. The first is a normalisation using the peak force magnitude ($\hat{f} = J/\Delta t$) and the second instead uses just the magnitude of the impulse (J). In both forms, the modal mass (m_n) and modal frequency (ω_n) are also included in non-dimensionalising the response. The force-normalised peak displacement was calculated using Equation 22 which represents the ratio between the peak displacement and the quasi static displacement for the impulse force.

$$\delta_n^* = \frac{h_{\max,n} m_n \omega_n^2 \Delta t}{J} = \frac{h_{\max,n} m_n \omega_n^2}{\hat{f}} \tag{22}$$

Fig. 17 shows the force-normalised peak displacement as a function of the dimensionless force duration. In this form, the shape of the curve is independent of the mode and depends only upon the damping ratio (ζ). As the force duration tends toward zero the impulse force magnitude tends toward infinity, as does the quasi static displacement. Therefore, the force-normalised peak displacement tends toward zero. As demonstrated by Fig. 15, the system response tends towards step response behaviour as the force duration increases relative to the modal frequencies and the response is limited by the step response overshoot ratio, as given by Equation 23:

$$\epsilon_n^* = \exp\left(\frac{-\pi\zeta_n}{\sqrt{1-\zeta_n^2}}\right) \tag{23}$$

The force-normalised peak displacement can then be approximated for long force durations using Equation 24:

$$\delta_{step,n}^* = 1 + \epsilon_n^* \tag{24}$$

A step response for an undamped system ($\zeta = 0$) has an overshoot ratio of 1 and a force-normalised peak displacement of 2. That is, the dynamic peak displacement is twice the quasi static as the system oscillates about the new equilibrium point with constant amplitude equal to the change in equilibrium position. For this reason the force-normalised peak displacement in Fig. 17 asymptotically approaches 2 as the force duration increases. In a system

with critical damping ($\zeta = 1$) the overshoot is zero and the dynamic peak displacement is equal to the quasi static peak displacement. For modes with low damping ratios the peak displacement can be approximated well using the step response approximation once the force duration exceeds half the modal period, $\tau_n > 0.5$. As the damping ratio increases towards critical damping ($\zeta_n = 1$) the force duration must exceed the modal period ($\tau_n > 1$) before the step response approximation can be used to describe the peak displacement. In all cases, the step response approximation overestimates the displacements for short durations. Bishop and Price (1979) quote damping factors ranging from 0.005 to 0.073 which is equivalent to a damping ratio range of 0.0025 to 0.037. For wave piercing catamarans, Thomas (2008) reported decay coefficients up to 0.14 which is equivalent to a damping ratio of 0.07. With such small damping ratios the step response approximation is appropriate for hull structures once the force duration exceeds half a modal period. In this case the response magnitude is limited by the maximum rate of change in the forcing term (Clough and Penzien, 1993).

In non-dimensionalising the displacement response by the peak force magnitude, the response for long force durations was easily observed. However, the response for short force durations was not. The second dimensionless form is the impulse-normalised peak displacement, Equation 25, in which the force duration is not used:

$$\eta_n^* = \frac{h_{max,n} m_n \omega_n}{J} \tag{25}$$

The impulse-normalised peak displacement ($h^*_{\mathrm{max},n}$) is the ratio between the actual displacement response and the displacement response to a Dirac delta impulse of the same magnitude, J. Fig. 18 shows that in this form the reduction in displacement response due to the increase in force duration can be seen directly. Again, the curve is only dependant on the damping ratio and not the mode. An impulse response approximation and a step response approximation of the impulse-normalised peak displacement is also included as given by Equations 26 and 27 respectively, where ϵ_n^* is the overshoot given by Equation 23:

$$\eta^*_{\mathrm{impulse},n} = \exp\left(\frac{-\zeta_n}{\sqrt{1-\zeta_n^2}} \operatorname{atan}\left(\frac{\sqrt{1-\zeta_n^2}}{\zeta_n}\right)\right) \tag{26}$$

$$\eta^*_{\text{max,step},n} = \frac{1+\epsilon^*_n}{\omega_n \Delta t} \quad (27)$$

For the special case of $\zeta = 1$, the impulse response approximation of Equation 23 is undefined. However, by taking the limit as $\zeta \to 1$ it can be shown that the response magnitude is given by Equation 28:

$$\eta^*_{\text{impulse},n}(\zeta_n = 1) = \exp(-1) \quad (28)$$

Both the impulse and step response approximations provide over-estimates of the modal response. As was the case for the force-normalised peak displacement, the reduction in response follows the step response approximation exactly for long force durations. As the total impulse was held constant in the analysis, the reduction in displacement response for long forces is solely related to the reduction in peak force which was required to maintain a constant total impulse as the force duration was increased. This reflects that the step response is limited by the percentage overshoot. The transition from impulse response to step response is critical to the type of analysis method that should be applied. If the forcing is impulsive for a given mode then the response of that mode to the forcing is governed by the magnitude of the applied impulse. However, if the forcing is not impulsive then the response is dependent on the transient form of the force term. Thus, the force distribution in time is critical for long duration forces, but not for short duration events.

As specified by Equation 21, an increase in the dimensionless force duration, τ_n, can be due to either an increase in the force duration or an increase in the modal frequency. Thus, for constant force duration the horizontal axis can be interpreted as a frequency axis. The Fourier transform of a rectangular pulse is superimposed on the impulse-normalised peak displacement in Fig. 19. The frequency spectrum is not smooth, tending to zero at integer values of dimensionless time, and the impulse-normalised peak displacement forms an upper bound on the spectrum. The frequency spectrum represents the average magnitude at a given frequency over the entire signal and does not capture local peaks in the signal. This is contrary to the impulse-normalised peak displacement which captures only the peak in the response. For example, mode four in Fig. 15 has a large peak displacement, but would be near one of the local minima in the frequency spectrum. Thus, this mode may not be represented in the frequency spectrum allowing one to conclude it was not strongly excited, when in fact it participated significantly in the response. For

structural design, both measures of the response are necessary. The peak displacement should be used to form the peak bending load case, while the frequency spectrum would be more appropriate for fatigue analysis.

The reduced displacement response of a system for increased force duration with constant total impulse can thus be attributed to two fundamental causes. The initial reduction results from reduced bandwidth of the impulsive excitation force. Then, as the impulse duration becomes long the response transitions to a step response and the displacement response reduces due to the reduced peak force while maintaining the same overshoot ratio.

The modal displacement response of the structure underpins the structural loads but, as was shown earlier, using the displacement response as the sole metric for modal participation can lead to significant error when determining appropriate truncation of a modal solution. As the modal displacement response is related to the modal vertical bending moment through the second spatial derivative (or curvature) of the mode shape, small displacements can yield large bending moments if the curvature of that mode is high.

The vertical bending moment resulting from a slam load on the 112 m INCAT wave piercing catamaran was investigated directly. For the 112 m INCAT wave piercing catamaran, the typical slam occurs during arch filling near the centre bow truncation. As specified in Table 2 the slam duration and location considered are 0.15 s and 90.7 m from the transom respectively. The peak vertical bending moment was calculated for a rectangular pulse at the dominant slam location for durations up to 0.25 s using truncation numbers of 3, 6, 9 and 12; corresponding to 1, 4, 7 and 10 vertical bending modes respectively. As shown in Fig. 20, the higher order modes contribute significantly to the vertical bending moments for short durations, but as the force duration is increased the fundamental mode becomes dominant. Once the force duration exceeds 0.07 s, the contributions from the higher order modes are significantly reduced. Since the duration of actual slams recorded in sea trials is approximately 0.15 s we see that it is the fundamental bending mode (mode 3) which dominates the peak hull bending moment for the 112 m INCAT hull. Also included in Fig. 20 is the experimentally identified vertical bending moment extrapolated from model scale Lavroff et al. (2011) which is approximated well by the uniform beam model. As the duration of the experimental slam event is not known to high accuracy it is shown over the estimated range.

The predicted peak vertical bending moment for a slam duration of 0.15 s is presented in Fig. 21 as a function of the truncation number (N); note that a greatly expanded ordinate scale has been used on the vertical axis. The peak vertical bending moment can be seen to converge after inclusion of 15 modes to 564 MNm, 17% larger than the bending moment extrapolated from model scale experiments (Lavroff, 2009b) presented in Table 2. The

contribution from the higher order modes to the peak bending moment is relatively small and the estimated peak bending moment using only one bending mode ($N = 3$) is only 5.5% less than that estimated using 15 modes or more.

The observed dominance of the fundamental bending mode can be shown using the impulse-normalised displacement response. The modal frequencies of modes 1 to 5 were non-dimensionalised using the slam duration of 0.15 s and are marked on the impulse-normalised peak displacement curve in Fig. 22 for the modelled damping ratio of 0.05. Here the dominance of the fundamental mode can be understood immediately. The responses of the rigid body heave and pitch modes is not significantly reduced and they respond as if the slam was a Dirac delta function. The response of the fundamental bending mode ($n = 3$) is only reduced by 21%, while the response of the second and higher bending modes ($n \geq 4$) are reduced by more than 68%. As the relative peak displacement scales the response of each mode to its impulse response, it provides a better estimate of the modal participation than the overall displacement response. Moreover, the dimensionless force durations for modes 4 and 5 are very close to whole integer values. Thus modes 4 and 5 will have a similar response to that of mode 4 in Fig. 15 where the peak response is significantly greater than the following whipping vibration of that mode. Consequently, these modes may be difficult to identify by spectral analysis.

Although the peak bending moment was estimated well using one flexural mode, this does not guarantee that the bending moment distribution could also be estimated well. Fig. 23 shows the moment distribution at the time of peak bending moment for truncation numbers of three and fifteen (dashed and chain lines respectively) as well as the local peak bending moment over the complete time record (solid line). The moment distribution has been expressed in these two ways as when more than one bending mode is considered the peak bending moment at a given longitudinal position on the hull generally does not occur at the same point in time as the peak moment at another position. Again, the peak bending moments identified at model scale by Lavroff et al. (2011) have been extrapolated to full scale and are included in the figure. The uniform beam model estimates are within 20.6% of the extrapolated model scale results for the aft bending moment and 5% for the forward bending moment, see Table 5. In the vicinity of the slam impact, the local bending moment at time of peak global bending moment is increased by 35% with inclusion of the higher order modes. If the local peak bending moment is considered, inclusion of the higher order modes results in larger moments over the entire hull length. The increase is most significant in the vicinity of the slam where the local peak bending moment is increased by 113%. In fact, the peak local bending

moment is increased over the entire length of the hull by inclusion of the higher order modes. Thus, although the higher order modes may not contribute significantly to the peak bending moment their influence in the slam region can be substantial. The present analysis does not consider two-way fluid structure coupling effects. Faltinsen (2000) states that "the significance of hydroelasticity increases with…increasing the value of the highest local natural period of the structure." It is therefore expected that the hydroelastic effects in the higher order modes are small.

6. Effect of Temporal Smoothing

So far the transient forces considered were rectangular pulses with sharp edges whereas slam forces, although short, cannot commence and terminate so abruptly. Clough and Penzien (1993) note that for long duration forces the response magnitude is related to the maximum rate of change in the forcing term. The effect of the edge sharpness on the modal response and vertical bending moment was qualitatively investigated by progressively smoothing the commencement and termination of the slam force using the cosine function to shape the transition while maintaining a constant total impulse, $J = \int f\, dt$. A ramping fraction, r, was defined using Equation 29:

$$r = \frac{\Delta t_r}{\Delta t} \tag{29}$$

where Δt_r is the time taken to ramp the force up or down. Thus, a ramping fraction of 1 yields a completely smooth force with an effective duration of Δt and a total duration of $2\Delta t$. Smoothed forces with ramping fractions of 0.4, 0.7 and 1 are considered here. The applied smoothed forces are shown in Fig. 24. The modal displacement responses of modes 3, 4 and 5 are shown in Fig. 25. The effect of temporal smoothing is more pronounced as the mode number, and therefore modal frequency, increases. In all cases increased smoothing reduces the displacement response. Of the modes presented, the most noticeable difference occurs for mode 5, in which vibration at the modal frequency is almost eliminated resulting in the response tracking the slam force in a quasi-static manner.

The peak vertical bending moment, that is the peak moment over the hull length at a given point in time, is shown as a function of time in Fig. 26 for ramping fractions of 0, 0.4 0.7 and 1 as calculated using truncation numbers of 3 and 15. As the forcing is smoothed the significance of the higher order modes in the bending response is reduced,

tending towards a quasi-static response and eliminating the overshoot associated with sharp step changes. In such cases, the resonant frequency of the mode is no longer present in the system response and the maximum spectral component in the signal is determined by the spectral content of the forcing term. The bending moment distribution at time of peak bending moment and the local peak bending moment is shown for a ramping fraction of $r = 1$ in Fig. 27. With a smooth forcing function the correlation to the model scale tests (Lavroff et al., 2011) is improved with a maximum discrepancy of 7.6%, see Table 6. Inclusion of the higher order modes results in a marginally increased peak bending moment. As was the case for the rectangular pulse the peak bending moment occurring in the region of the slam impact is significantly under estimated when the high order modes are neglected. As the response of the higher order modes is reduced to quasi-static behaviour the effect of these modes on the bending moment distribution can be considered by quasi-static analysis.

7. Conclusion

The effect of impact duration and temporal smoothing of a slam force has been investigated using a beam model representative of a wet ship system. The analysis was conducted on a modal basis and the effect of truncating the solution at a finite number of nodes considered. A uniform beam on elastic foundation was used as a representative model of the wet ship system to minimise computational effort. Despite the limitations of the model, the predicted peak bending moment for the 112 m INCAT catamaran was found to agree well with experimental data: using an estimated slam duration of 0.15 s the predicted bending moments deviated from experimental results by a maximum of 7.6%. The effect of spatial slam force distribution has not been addressed and may be considered in future work.

The global displacement response was found to be a poor indicator of modal convergence. In the case of a Dirac delta impulse, the displacement response converged quickly as the truncation number was increased while the bending moment response did not converge. The significance of the higher order modes was most pronounced in the region near the impact force where the inclusion of higher order modes significantly increased the peak bending moment. The resulting high frequency components are easily observed in the transient bending moment near the impact location but only weakly observable for more remote measurements. Although spectral analysis can aid in identifying the higher order modes, the perceived magnitude may still be under estimated as the spectral content of the response is limited by that of the excitation. It has been shown that as many as 15 flexural modes may be

necessary to correctly predict the bending moment distribution in the region of the slam, but quasi static treatment may be acceptable in the case of smooth forces for modes with dimensionless force durations greater than 1.

As expected, the vertical bending moment was found to reduce with increasing force duration as a result of distributing the energy input over time and thus reducing peak forces. This highlights a significant benefit of the INCAT centre bow which acts to lengthen the duration of the slam impact. It can therefore be expected that higher order modes would be more significant in other high speed catamarans which do not employ such a means of temporally lengthening the slam impulse. The impulse-normalised peak displacement was introduced as a metric to enable the reduction in modal response due to the duration of an impact to be estimated. As this metric considers each mode in isolation it is not subject to the limitations of the global displacement response. For impacts with durations less than half a modal period it has been shown that the temporal distribution of the slam force has little significance and the total impulse determines the modal response. However, in order to properly model the effects of the higher order modes, the temporal distribution of the slam force must be known.

Temporal smoothing of the slam force was found to further reduce the participation of the higher order modes. However, they still acted to increase the bending moment in the region of the slam. For temporally smooth forces the effect of the higher order modes can be well approximated by quasi-static methods. If the forcing term is non-smooth, then the response of the higher order modes can be better estimated using a step response approximation as overshoot is present.

8. Acknowledgements

This work has been supported by INCAT Tasmania Pty Ltd, Revolution Design Pty Ltd, the Australian Research Council, the University of Tasmania and the Australian Maritime College.

9. References

Amin, W., 2009. Non-linear Unsteady Wave Loads on Large High-Speed Wave Piercing Catamarans, Ph.D. Thesis, University of Tasmania.

Amin, W., Davis, M.R., Thomas, G.A., and Holloway, D. S., 2009. Slamming Quasi-Static Analysis of an INCAT 98m High-Speed Wave Piercing Catamaran, Innovations in High-Speed Marine Vessels.

Amin, W., Davis, M. R., Thomas, G., and Holloway, D. S., 2014. Transient Wave Loads on Large High-Speed Catamarans, Proceedings of the 8th International Conference of High-Performance Marine Vehicles. Duisberg.

Bishop, R. E. D. and Price, W. G., 1979. Hydroelasticity of ships, Cambridge University Press, Cambridge.

Castiglione, T., Stern, F., Bova, S., and Kandasamy, M., 2011. Numerical Investigation of the Seakeeping Behavior of a Catamaran Advancing in Regular Head Waves. Ocean Engineering, 38, 16, 1806–1822.

Cheung, K. F., Siedl, L. H., and Wang, S., 1998. Analysis of SWATH ship structures, Marine Technology and SNAME News, 35, 2, 85–97.

Clough, R. W., and Penzien, J., 1993, Dynamics of Structures, 2nd ed., McGraw-Hill, New York.

Das, S. and Cheung, K. F., 2012. Hydroelasticity of Marine Vessels Advancing in a Seaway, Journal of Fluids and Structures, 34, 271-290.

Dessi, D. and Mariani, R., 2008. Analysis and Prediction of Slamming-Induced Loads of a High-Speed Monohull in Regular Waves, Journal of Ship Research, 52, 1, 71-86.

DNV (Det Norske Veritas) , 2011. Rules for Classification of High Speed, Light Craft and Naval Surface Craft. Part3, Chapter 9.

Faltinsen, O. M., 2000. Hydroelastic slamming, Journal of Marine Science and Technology, 5, 49-65.

Faltinsen, O. M., Landrini, M. and Greco, M., 2004. Slamming in Marine applications, Journal of Engineering Mathematics, 48, 187-217.

French, B., 2012. Slamming of Large High-Speed Catamarans in Irregular Seas, PhD Thesis, University of Tasmania.

Ge, C., Faltinsen, O.M., and Moan, T., 2005. Global Hydroelastic Response of Catamarans Due to Wetdeck Slamming, Journal of Ship Research, 49, 1, 24-42.

Jang, C. D., Jung, J. J. and Korobkin, A. A., 2007. An approach to estimating the hull girder response of a ship due to springing, Journal of Marine Science and Technology, 12, 95-101.

Kapsenberg, G. K., and Brizzolara, S., 1999. Hydro-elastic Effects of Bow Flare Slamming on a Fast Monohull, 5th International conference on Fast Sea Transportation, Seattle, 699-708.

Kapsenberg, G. K., 2011. Slamming of Ships: Where are We Now?, Philosophical Transactions of the Royal Society A, 369, 2892-2919.

Lavroff, J., Davis, M. R., Holloway, D. S., and Thomas, G., 2009. The Vibratory Response of High-Speed Catamarans to Slamming Investigated by Hydroelastic Segmented Model Experiments, International Journal of Maritime Engineering 151 (A4), 1–11.

Lavroff, J., 2009b. The Slamming and Whipping Vibratory Response of a Hydroelastic Segmented Catamaran Model, PhD Thesis, University of Tasmania.

Lavroff, J., Davis, M.R., Holloway, D.S., and Thomas, G.A., 2010. Slamming of High-Speed Catamarans in Severe Sea Conditions Investigated by Hydroelastic Segmented Model Experiments, Proceedings of the 28th Symposium on Naval Hydrodynamics, Office of Naval Research, 169–180.

Lavroff, J., Davis, M. R., Holloway, D. S. and Thomas, G., 2011. Determination of Wave Slamming Loads on High-Speed Catamarans by Hydroelastic Segmented Model Experiments, Transactions of the Royal Institute of Naval Architects, Part A3, International Journal of Maritime Engineering, 153, A185-A197.

Matsubara, S., 2011. Ship Motions and Wave-Induced Loads on High Speed Catamarans, PhD Thesis, University of Tasmania.

McGoldrick, R. T., 1960. Ship vibration, U.S. Government Printing Office, Washington.

Rao, S. S. 1995. Mechanical Vibrations, third edition, Addison-Wesley, Massachusetts, 531-532.

Schellin, T. E., and el Moctar, O., 2007. Numerical Prediction of Impact-Related Wave Loads on Ships, Journal of Offshore Mechanics and Arctic Engineering, 129, 39-47.

Senjanović, I., Malenica, Š and Tomašević, S., 2009. Hydroelasticity of Large Container Ships, Marine Structures, 22, 287-314.

Shahraki, J., 2014. The Influence of Hull Form on the Slamming Behaviour of Large High Speed Catamarans, PhD Thesis, University of Tasmania.

Thomas, G. A., Davis, M. R., Holloway, D. S. and Roberts, T. J., 2003. Transient Dynamic Slam Response of Large High Speed Catamarans, 7th International conference on Fast Sea Transportation, Ischia, Italy.

Thomas, G., Davis, M., Holloway, D. and Roberts, T., 2008. The Vibratory Damping of Large High-speed Catamarans, Marine Structures, 2, 1–22.

Tuitman, J. T., Malenica, Š., and van't Veer, R., 2012. Generalized Modes in Time-Domain Seakeeping Calcualtions, Journal of Ship Research. 56, 4, 215-233.

Waltham, C., and Kotlicki, A., 2009. Construction and Calibration of an Impact Hammer, American Journal of Physics, 77, 10, 945–949.

10. Figures

Fig. 1: Hull 064 - Natchan Rera. A 112m INCAT high speed wave piercing catamaran (image courtesy of INCAT Tasmania Pty Ltd).

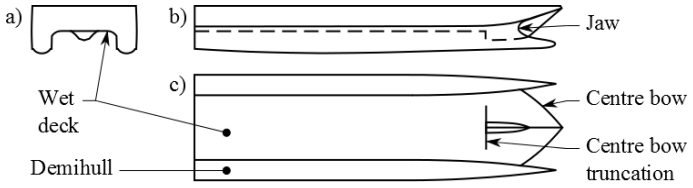

Fig. 2: Geometric features of a wave piercing catamaran: a) body section; b) profile view; c) plan view.

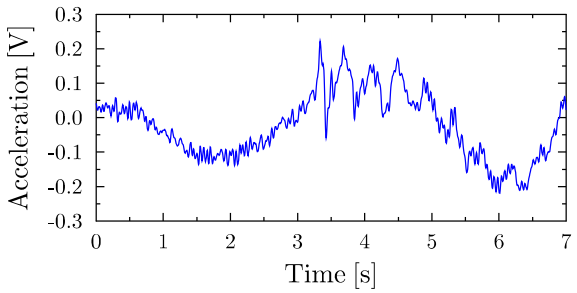

Fig. 3: Acceleration measured at the bow of Hull 064 during a slam event while crossing the Bass Strait, low pass filtered at 17 Hz (Lavroff et al., 2009).

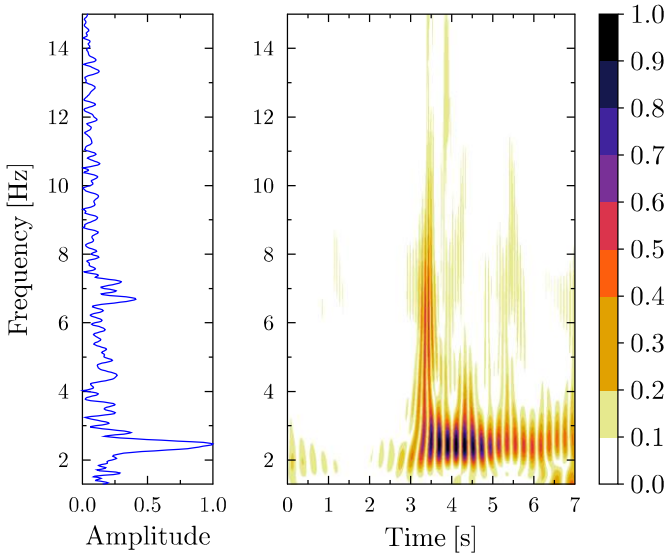

Fig. 4: Fourier transform (left) and continuous wavelet transform (right) of the slam signal in Fig. 3 showing vibration at frequencies higher than the fundamental bending mode frequency of 2.5 Hz.

Fig. 5: Formation of jet flows during the water entry of the centre bow on a 2.5m scale model of an INCAT wave piercing catamaran in 90mm waves at a forward speed of 1.53 m/s (Lavroff, J., 2009b).

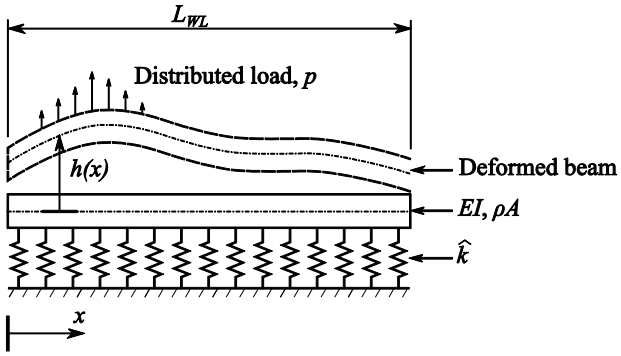

Fig. 6: Schematic of the continuous beam model implemented to analyse the effects of temporal force duration on the modal response.

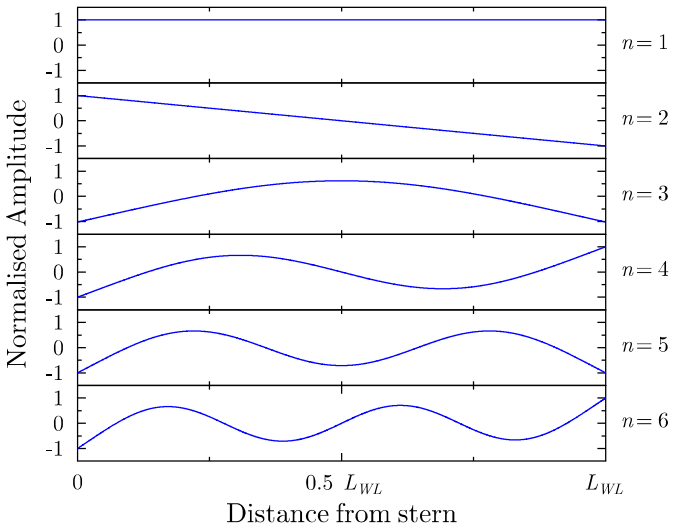

Fig. 7: First six mode shapes of the continuous beam system including: rigid body heave (n = 1), rigid body pitch (n = 2), first longitudinal bending (n = 3); and higher longitudinal bending modes (n > 3).

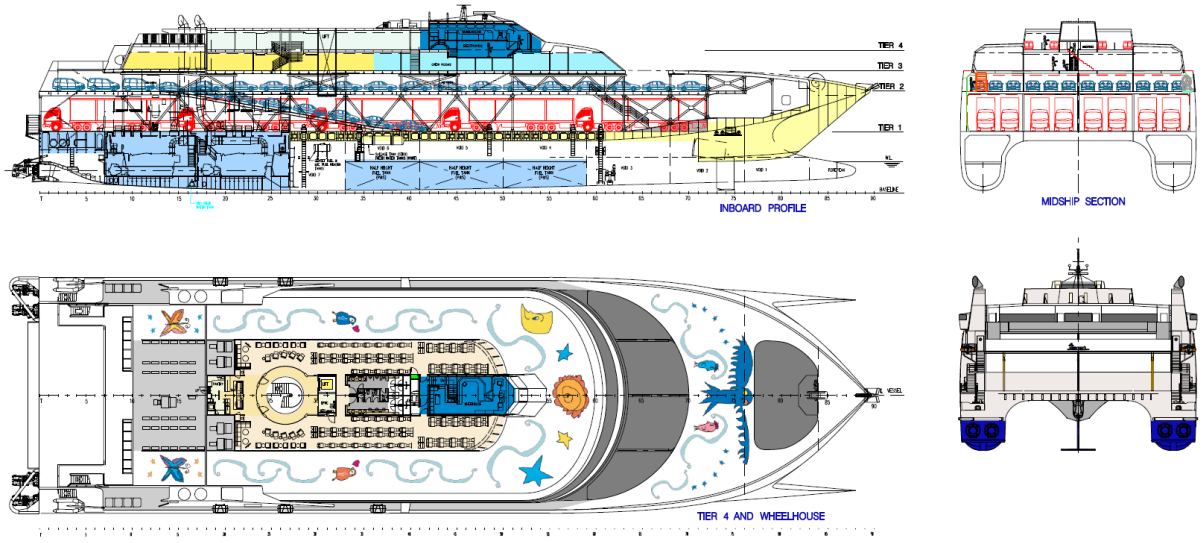

Fig. 8: General arrangement of Hull 064, Natchan Rera (image courtesy of INCAT Tasmania Pty Ltd).

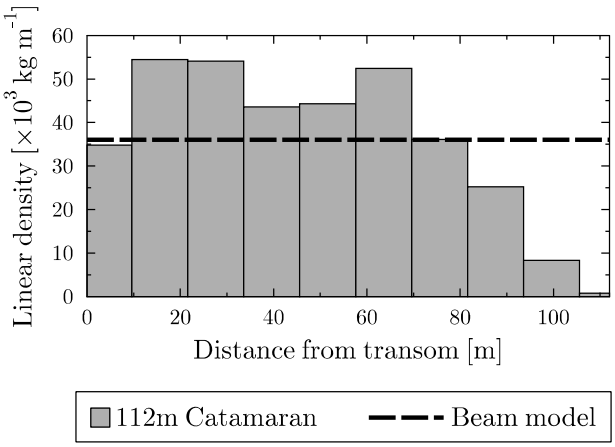

Fig. 9: Estimated mass distribution from finite element analysis for hull 064 (112 m catamaran) and the uniform distribution used in the beam model.

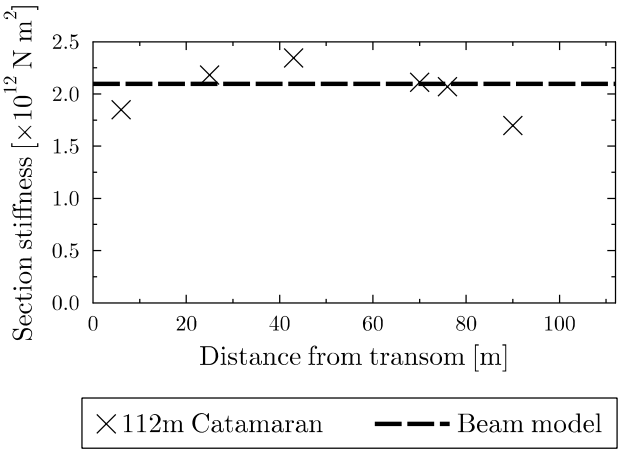

Fig. 10: Estimated stiffness distribution from finite element analysis for six locations on hull 064 (112m catamaran) and the uniform distribution used in the beam model.

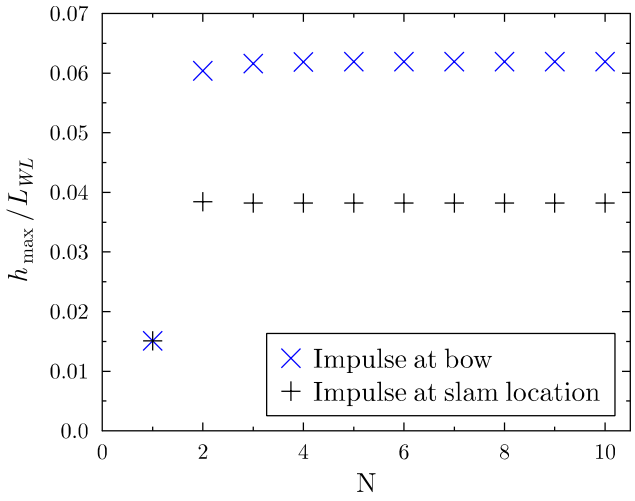

Fig. 11: Calculated peak displacement (h_{max}) divided by waterline length (L_{WL}) as a function of the number of modes considered (N) in response to a Dirac delta impulse of 9 MNs applied at the bow and the dominant slam location.

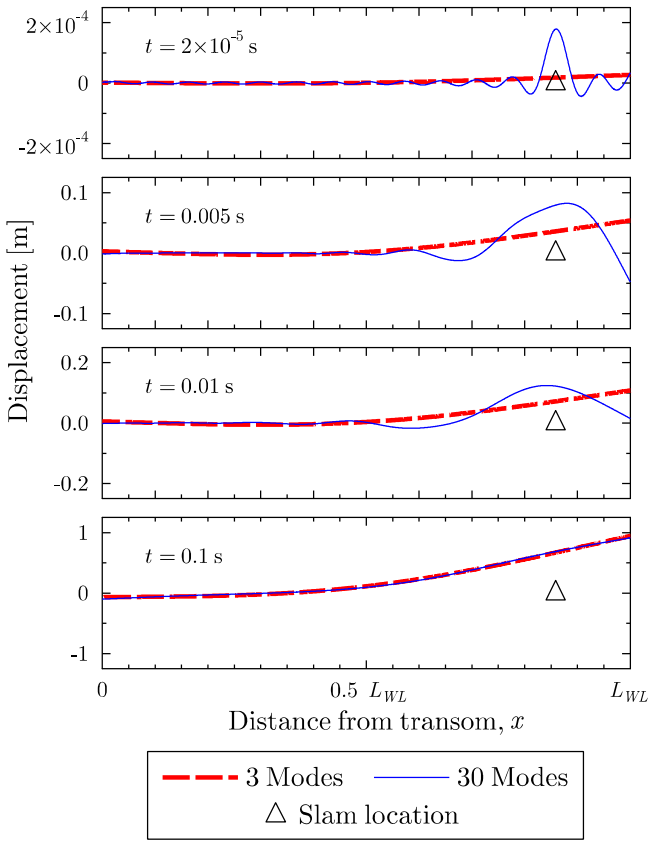

Fig. 12: Calculated beam deformation using three modes (N=3) and thirty modes (N=30) following a Dirac delta impulse at the dominant slam location.

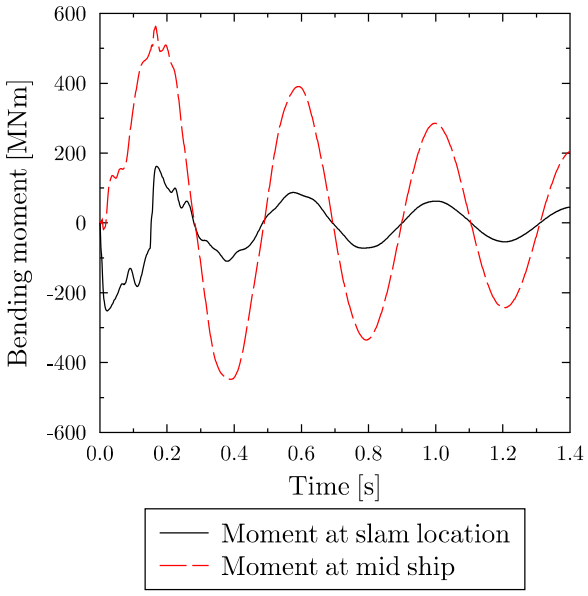

Fig. 13: Transient bending moment at the slam location and mid ship for a truncation number of N=15. The higher frequency components are more readily identified in the measurement at the slam location.

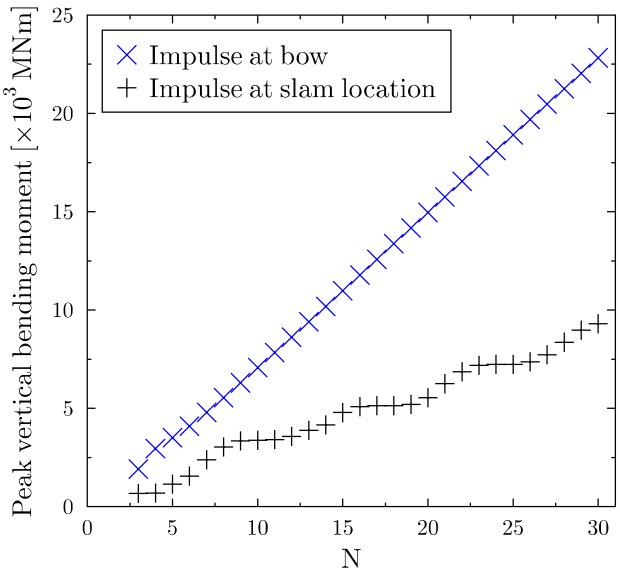

Fig. 14: Calculated peak bending moment as a function of the number of modes considered (N) in response to a Dirac delta impulse of 9 MNs applied at the bow and the dominant slam location.

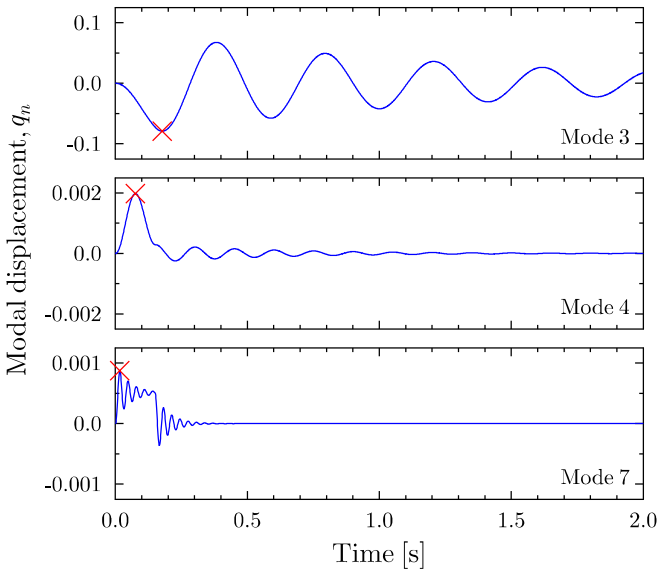

Fig. 15: Modal displacement responses of modes 3, 4 and 7. The response of mode 3 is characteristic of an impulse response while the response of mode 7 is characteristic of consecutive step responses. The response magnitude of the higher modes is decreased.

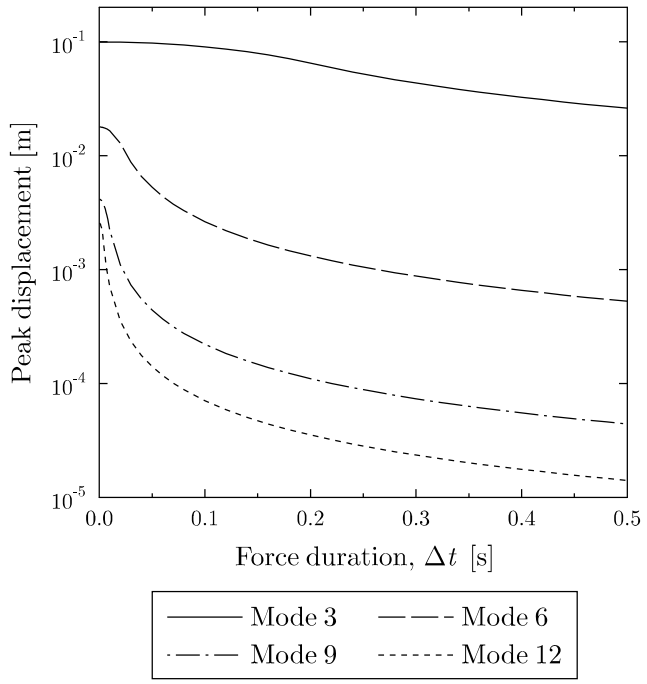

Fig. 16: Peak displacement in the transient modal response for modes 3, 6, 9 and 12. As the force duration is increased the peak displacement of all modes is decreased, but at higher rates for the higher order modes.

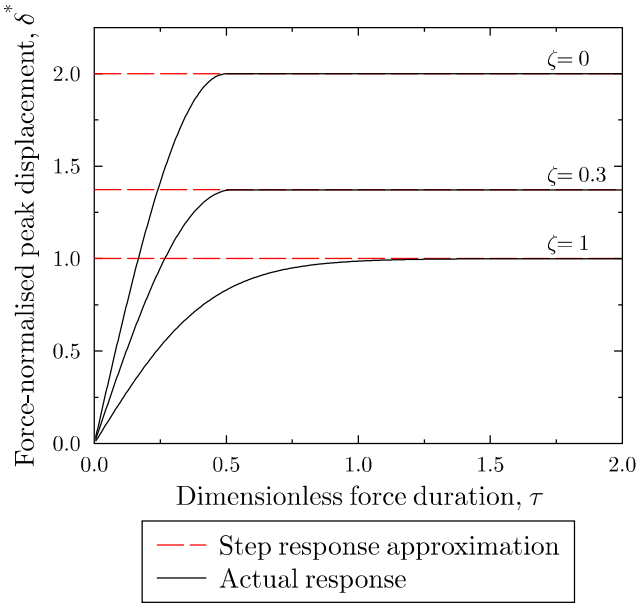

Fig. 17: Force-normalised peak displacement as a function of dimensionless force duration for damping ratios, ζ, of 0, 0.3 and 1.

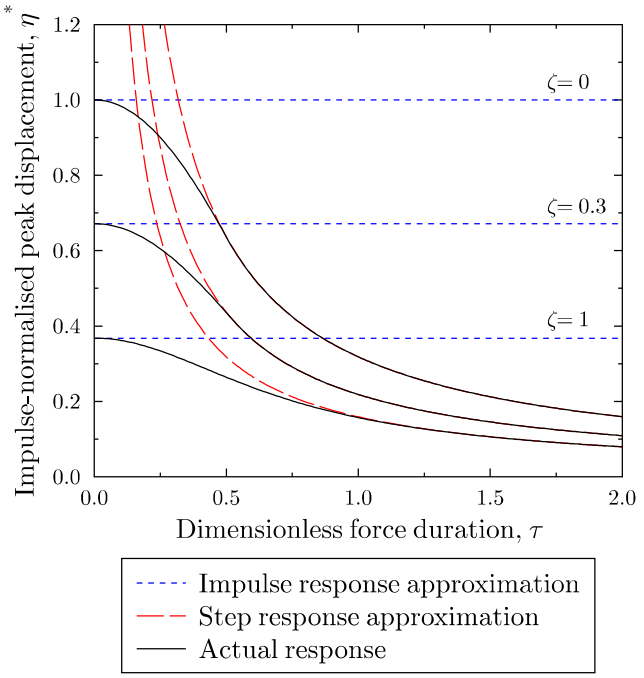

Fig. 18: Impulse-normalised peak displacement as a function of dimensionless force duration for damping ratios, ζ, of 0, 0.3 and 1.

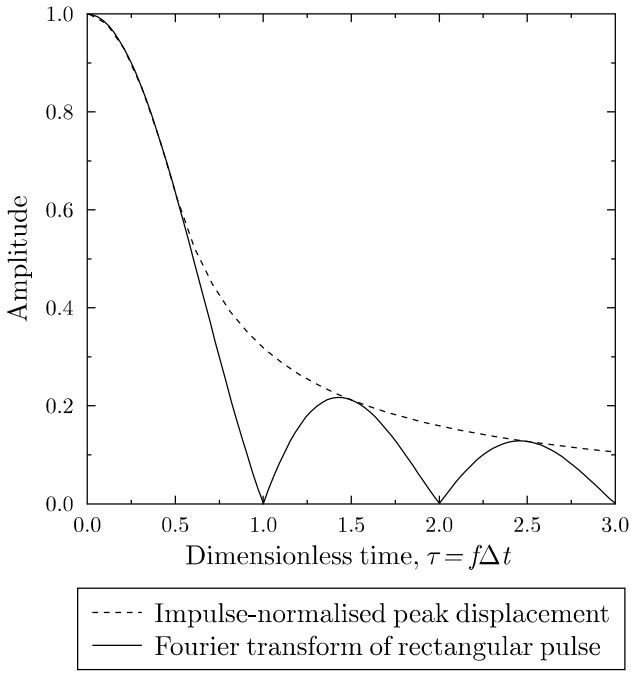

Fig. 19: Impulse-normalised peak displacement for an undamped system compared to the scaled frequency spectrum of a rectangular pulse calculated using Fourier transform.

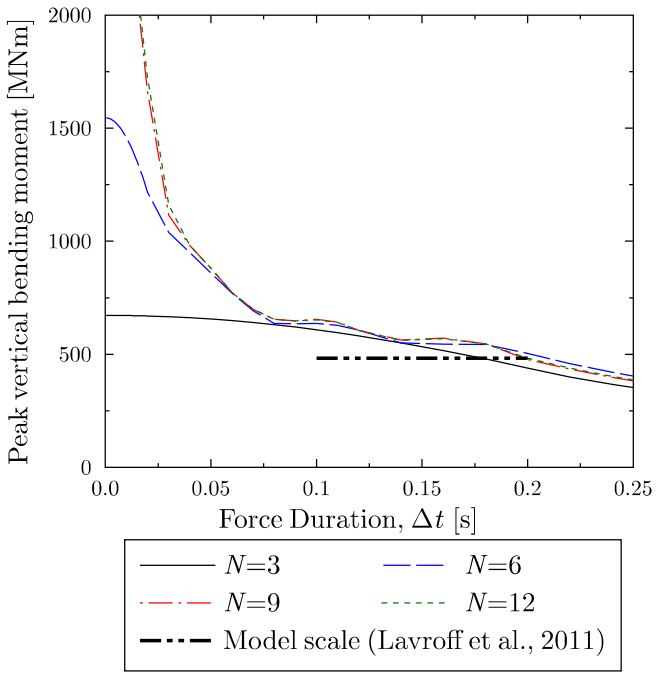

Fig. 20: Peak vertical bending moment as a function of force duration in response to an impact at the dominant slam location (90.7 m forward of transom) using 3, 6, 9 and 12 system modes in the truncated analysis.

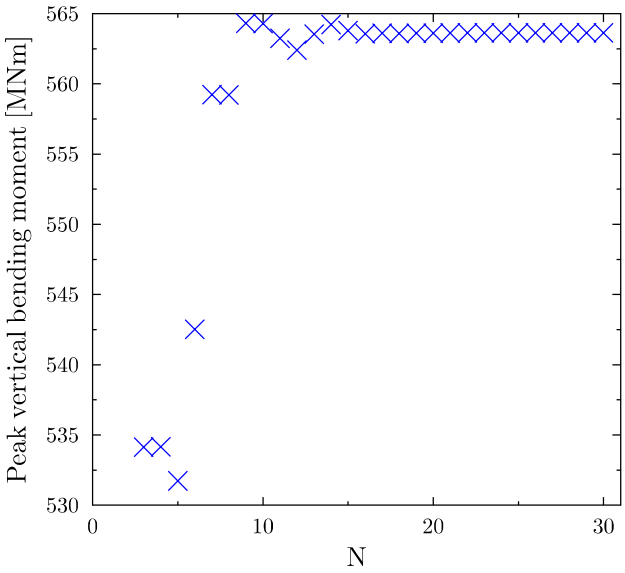

Fig. 21: Calculated peak bending moment as a function of the number of modes considered (N) resulting from a square pulse with duration 0.15s and impulse magnitude of 9 MNs applied at the dominant slam location.

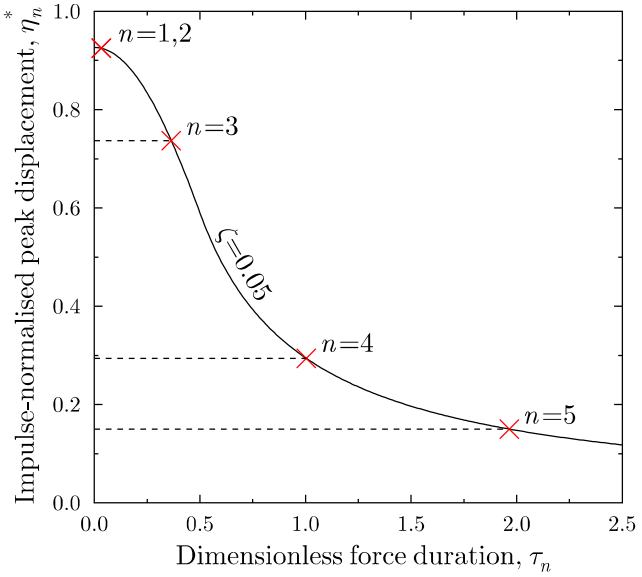

Fig. 22: Impulse-normalised peak displacement for the first 5 system modes. The response of modes 4 and 5 are significantly reduced due to the duration of the applied force.

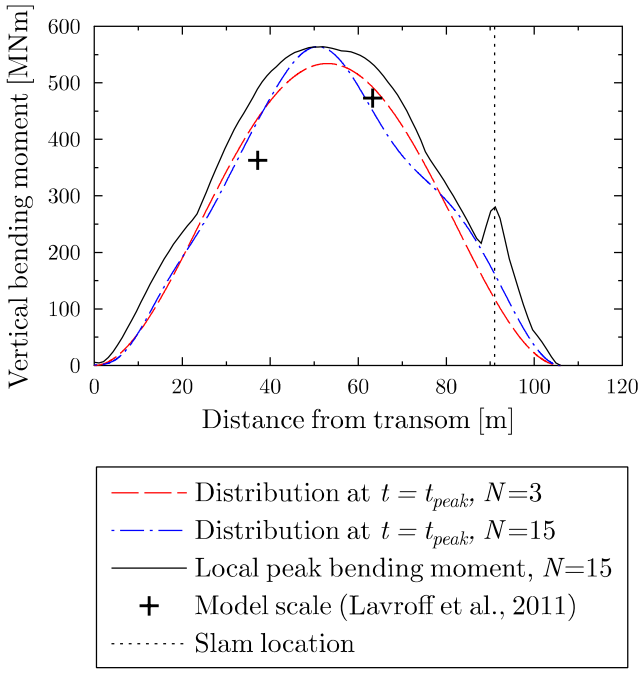

Fig. 23: Vertical bending moment distribution for analysis using one bending mode ($N = 3$) and thirteen bending modes ($N = 15$) for a rectangular pulse.

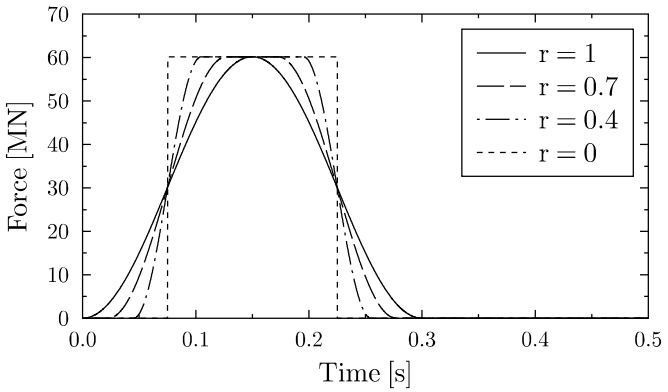

Fig. 24: Transient forcing function for temporally smoothed forcing functions with ramping fractions of $r = 0, 0.4, 0.7$ and 1.

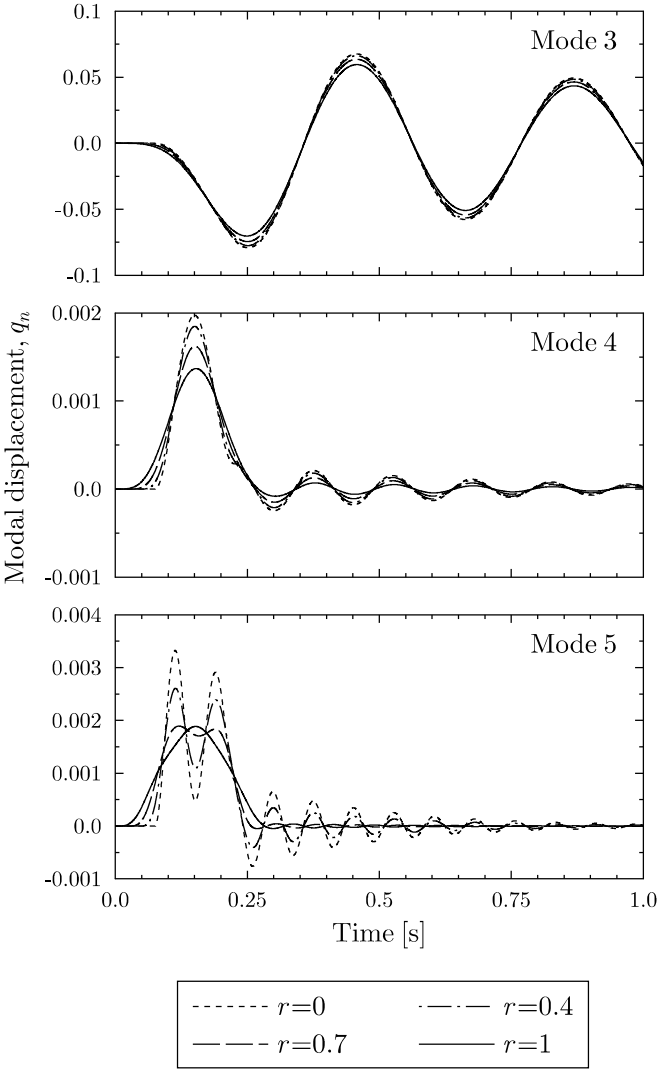

Fig. 25: Response of modes 3, 4 and 5 to a force with ramping fractions of $r = 0, 0.4, 0.7$ and 1 with an effective duration of 0.15s.

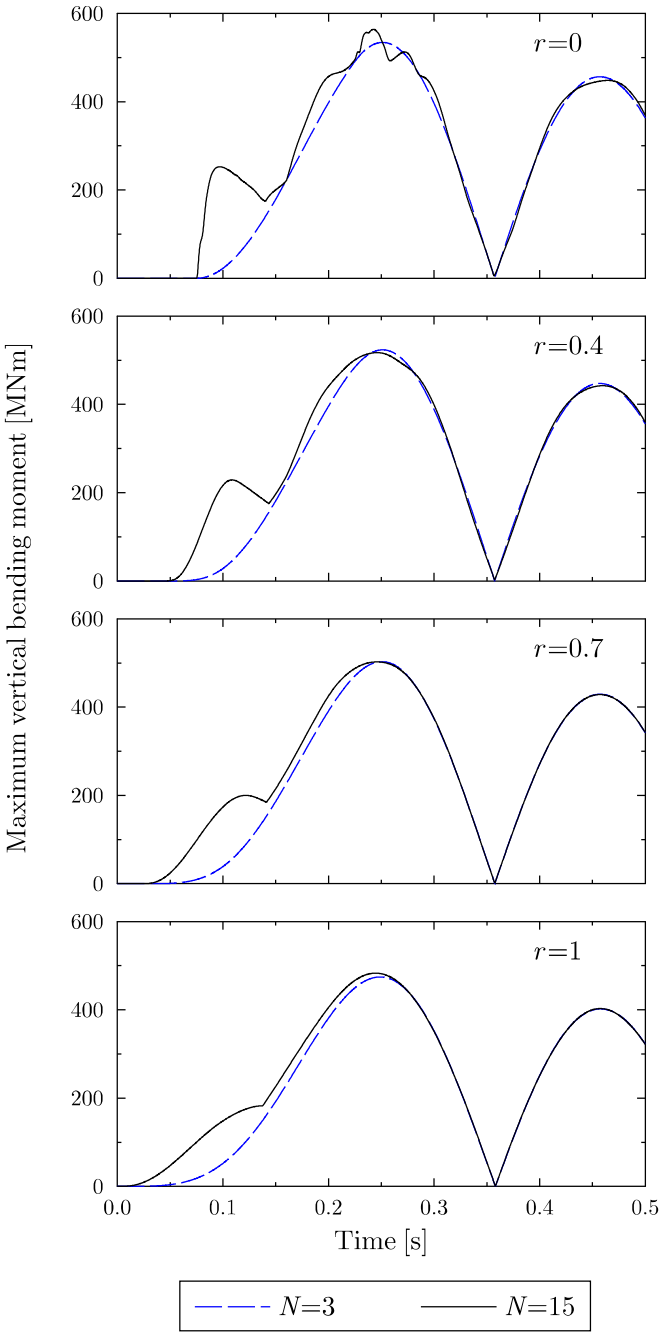

Fig. 26: Transient peak vertical bending moment using truncation numbers of 3 and 15 for ramp fractions of 0 (representing a rectangular force pulse), 0.4, 0.7 and 1 (representing continuous a smooth force pulse).

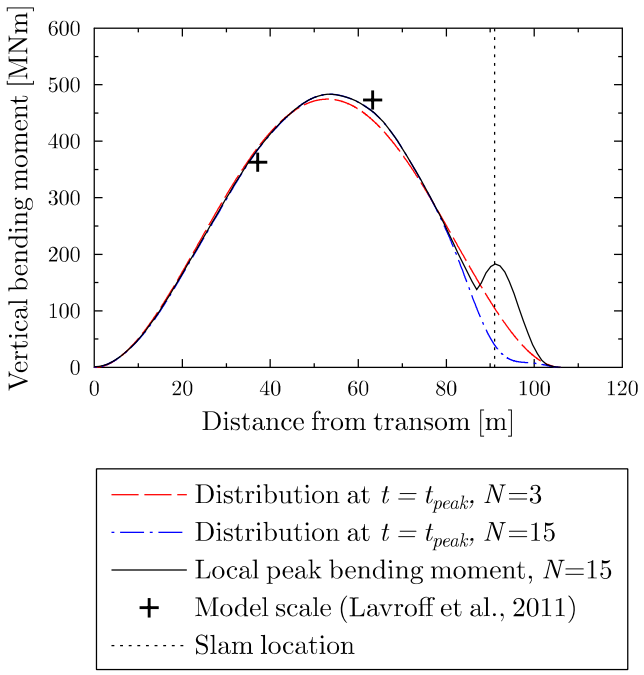

Fig. 27: Vertical bending moment distribution for analysis using one bending mode ($N = 3$) and thirteen bending modes ($N = 15$) for a smooth impulse ($r = 1$).

11. Tables

Table 1: Comparison of mass, stiffness and overall slam duration of a wave piercing INCAT catamaran to those of several monohull vessels.

	Length, L [m]	2-node vertical bending frequency, f_3 [Hz]	Second moment of area, I [m^4]	Displacement, m_v [t]	I/L^4	m_v/L^3 [kg m^{-3}]	Slam Duration [s]
112m INCAT catamaran[1]	112†	2.4	35	2200*	2.2×10^{-7}	1.56	0.15
7800 TEU container ship[2]	334†	0.49	700	135336*	5.6×10^{-8}	3.63	-
High speed monohull[3]	128‡	1.35	13	3908	4.8×10^{-8}	1.86	1.6
146m High speed monohull[4]	145.6†	1.1	-	-	-	-	1.3
Offshore supply vessel[5]	130‡	-	-	5470	-	2.4	1.2
† Length overall		‡ Length between perpendiculars			* At full load		
[1] Lavroff, 2009b [2] Senjanović et al., 2009 [3] Dessi and Mariani, 2008 [4] Kapsenberg and Brizzolara, 1999 [5] Schellin and el Moctar, 2007							

Table 2: Selected ship parameters for a 112m INCAT wave piercing catamaran

Overall length	112.5	m
Waterline length	105.6	m
Displacement	2209	t
First longitudinal bending frequency	2.44	Hz
Slam impulse †	9.0	MNs
Peak slam vertical bending moment †	483	MNm
Slam duration †	0.15	s
Slam location (from transom) †	90.7	m
Added mass	1507	t
† Extrapolated from model scale results (Lavroff, 2009b)		

Table 3: Ship parameters identified for the uniform beam model of a 112 m INCAT wave piercing catamaran.

Linear density, ρA	36×10^3	kg m^{-1}
Elastic base stiffness, $\hat{k}$	69×10^3	Nm^{-2}
Beam stiffness, EI	2.10×10^{12}	Nm^2

Table 4: Modal frequency estimates for a 112 m INCAT catamaran using the continuous beam model.

Mode Number n	Mode Description	Modal Frequency, f_n [Hz]
1	Heave	0.22
2	Pitch	0.22
3	First longitudinal bending	2.43
4	Second longitudinal bending	6.69
5	Third longitudinal bending	13.1
6	Fourth longitudinal bending	21.7

Table 5: Predicted peak vertical bending moments in response to a rectangular impulse with a duration of 0.15s compared to extrapolated model scale experimental data.

Location	Extrapolated model scale bending moment [NMm] †	Beam model ($N = 3$)		Beam model ($N = 15$)	
		Bending moment [NMm]	Error to model scale	Bending moment [NMm]	Error to model scale
Forward	473	492	4.1%	450	-4.8%
Aft	363	437	20.6%	432	19.3%
† Extrapolated from model scale results (Lavroff, 2009b)					

Table 6: Predicted peak vertical bending moments in response to a smooth impulse with a duration of 0.15s compared to extrapolated model scale experimental data.

Location	Extrapolated model scale bending moment [NMm] †	Beam model ($N = 3$)		Beam model ($N = 15$)	
		Bending moment [NMm]	Error to model scale	Bending moment [NMm]	Error to model scale
Forward	473	437	-7.6%	452	-4.4%
Aft	363	389	7.1%	385	6.1%
† Extrapolated from model scale results (Lavroff, 2009b)					